Acta Cryst E CRYSTALLOGRAPHIC COMMUNICATIONS

ISSN 2056-9890

Crystal structure of seladelpar, $C_{21}H_{23}F_3O_5S$, from synchrotron powder diffraction data and density functional theory

Jacob K. Salazar,[a] James A. Kaduk,[b,c]* Anja Dosen,[d] Megan Rost[d] and Thomas N. Blanton[d]

[a]North Central College, Department of Chemistry, 131 S. Loomis St., Naperville IL 60540, USA, [b]North Central College, Department of Physics, 131 S. Loomis St., Naperville IL 60540, USA, [c]Illinois Institute of Technology, Department of Chemistry, 3101 S. Dearborn St., Chicago IL 60616, USA, and [d]ICDD, 12 Campus Blvd., Newtown Square PA 19073-3273, USA. *Correspondence e-mail: kaduk@polycrystallography.com

Received 27 May 2026
Accepted 30 July 2026

Edited by W. T. A. Harrison, University of Aberdeen, United Kingdom

Keywords: powder diffraction; seladelpar; Livdelzi; Rietveld refinement; density functional theory.

CCDC references: 2577790; 2577791

Supporting information: this article has supporting information at journals.iucr.org/e

The crystal structure of seladelpar, $C_{21}H_{23}F_3O_5S$ [systematic name 2-(4-{(2*R*)-2-ethoxy-3-[4-(trifluoromethyl)phenoxy]propylsulfanyl}-2-methylphenoxy)acetic acid], has been solved and refined using synchrotron X-ray powder diffraction data, and optimized using density functional theory techniques. Seladelpar crystallizes in space group $P2_12_12_1$ and the molecule adopts a U-shaped conformation. The crystal structure is characterized by layers lying parallel to the *ab* plane. One classical O—H···O hydrogen bond links the carboxylic acid group and an ether O into chains propagating along the *b*-axis direction and the chains are consolidated by a weak C—H···S hydrogen bond.

1. Chemical context

Seladelpar, $C_{21}H_{23}F_3O_5S$ (marketed as Livdelzi, as the lysine dihydrate salt), is used to treat primary biliary cholangitis, an autoimmune disease of the liver (Shukla & Misra, 2025). The systematic name (CAS Registry Number 851528-79-5) is 2-[4-[(2*R*)-2-ethoxy-3-[4-(trifluoromethyl)phenoxy]propyl]sulfanyl-2-methylphenoxy]acetic acid.

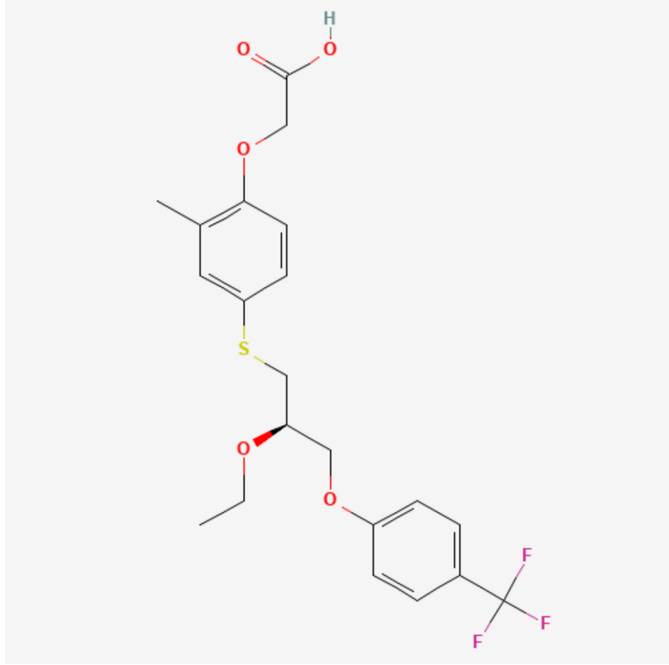

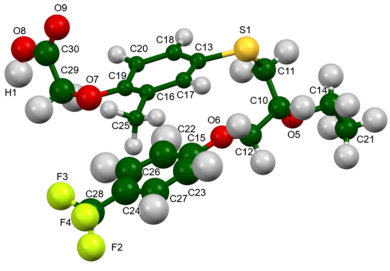

This work was carried out as part of a project (Kaduk *et al.*, 2014) to determine the crystal structures of large-volume

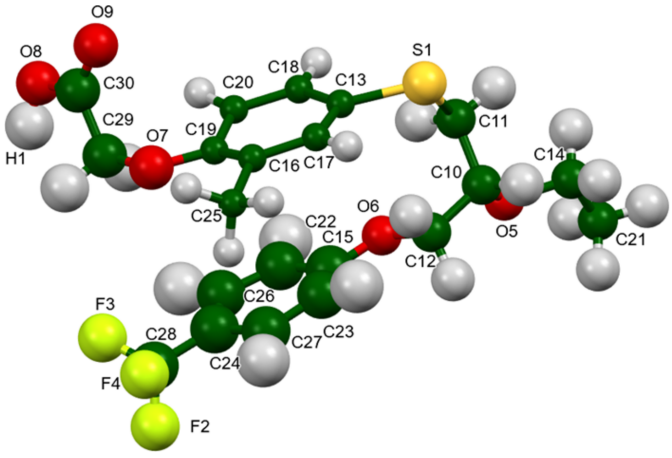

Figure 1
The molecular structure of seladelpar, based on the Rietveld refinement, with the atom numbering. The atoms are represented by 50% probability spheroids.

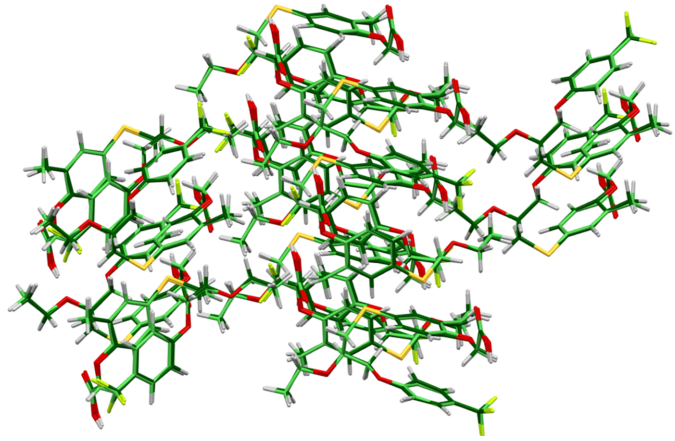

Figure 2
Comparison of the Rietveld-refined (colored by atom type) and *VASP*-optimized (pale green) structures of seladelpar, calculated using the *Mercury* CSD-Materials/Search/Crystal Packing Similarity tool. The root-mean-square Cartesian displacement is 0.139 Å.

commercial pharmaceuticals, and include high-quality powder diffraction data for them in the Powder Diffraction File (Kabekkodu *et al.*, 2024).

2. Structural commentary

The molecular structure of seladelpar is illustrated in Fig. 1. The root-mean-square difference of the non-H atoms in the Rietveld-refined and *VASP*-optimized structures, calculated using the *Mercury* (Macrae *et al.*, 2020) CSD-Materials/search/crystal packing similarity tool is 0.139 Å (Fig. 2); the structures are essentially identical. The root-mean-square Cartesian displacement of the non-H atoms in the refined and optimized structures, calculated using the *Mercury* Calculate/molecule overlay tool, is 0.112 Å (Fig. 3). The agreements are within the normal range for correct structures (van de Streek & Neumann, 2014). Given the normal representation of the molecule in an extended conformation, the bent solid-state conformation with the phenyl rings approximately parallel may be unexpected. The remaining discussion will emphasize the *VASP*-optimized structure.

Almost all of the bond distances, bond angles, and torsion angles fall within the normal ranges indicated by a *Mercury* Mogul geometry check (Macrae *et al.*, 2020). Only the torsion angles involving rotation about the S1—C13 bond are flagged as unusual. They lie in broad valleys of bimodal 0/180° distributions of similar torsion angles, so the conformation of the molecule is slightly unusual, but not unprecedented. The mean plane of the aromatic ring with the trifluoromethyl substituent corresponds approximately with the $(1\bar{1}2)$ Miller

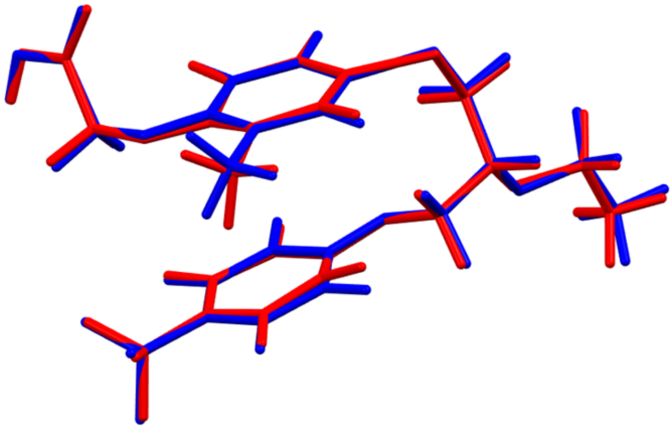

Figure 3
Comparison of the refined structure of seladelpar (red) to the *VASP*-optimized structure (blue). The comparison was generated using the *Mercury* Calculate/Molecule Overlay tool; the r.m.s. difference is 0.112 Å.

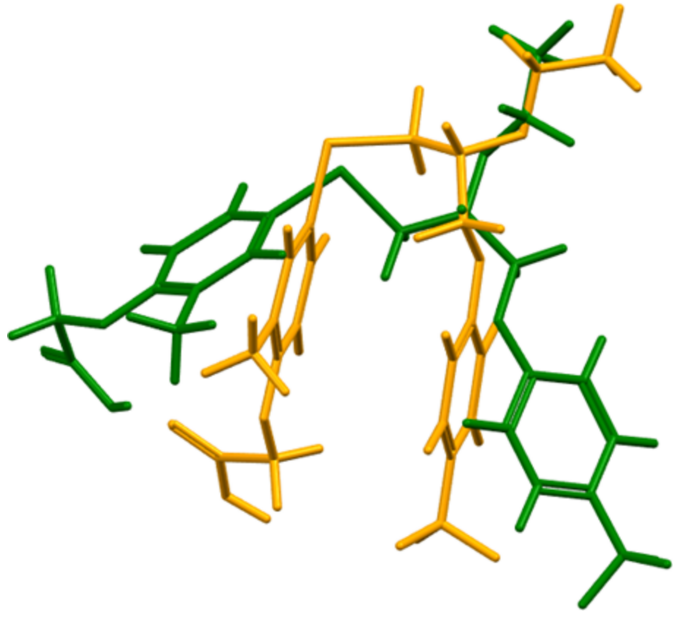

Figure 4
Comparison of the molecular structure of seladelpar determined here (orange) with that in PDB entry 8HUP (green). The root-mean-square difference is 2.801 Å.

Table 2
Hydrogen-bond geometry (Å, °).

D—H···A	D—H	H···A	D···A	D—H···A
O8—H1···O5^{i}	1.01	1.72	2.725	175
C23—H16···S1^{ii}	1.09	2.72	3.785	166

Symmetry codes: (i) $-x+1, y+\frac{1}{2}, -z+\frac{1}{2}$; (ii) $-x, y-\frac{1}{2}, -z+\frac{1}{2}$.

plane, and the mean plane of the other phenyl ring is approximately (11$\overline{1}$). The bent shape of the molecule is reflected in the normal S1—C11—C10—C12 (*gauche*) and O5—C10—C11—S1(*trans*) torsion angles (Table 1).

Quantum chemical geometry optimization of the isolated seladelpar molecule (DFT/B3LYP/6-31G*/water) using *Spartan '24* (Wavefunction, 2025) indicated that the observed conformation is 3.6 kcal mol^{-1} higher in energy than a local minimum, which has a similar overall shape (r.m.s. difference = 0.56 Å) but differences at the periphery of the molecule. The global minimum-energy conformation (MMFF force field) is 8.3 kcal mol^{-1} lower in energy, with a similar overall shape (r.m.s. difference = 1.76 Å) but with differences in the orientations of the carboxylic acid and trifluoromethyl groups. The conformation of seladelpar in the PDB entry 8HUP is very different from that observed here (Fig. 4; r.m.s. difference = 2.80 Å) and 1.4 kcal mol^{-1} lower in energy. Apparently, the molecule is flexible, and intermolecular interactions are important in determining the observed conformation.

3. Supramolecular features

The crystal structure (Fig. 5) is characterized by layers lying parallel to the *ab* plane. Parallel stacking of rings is apparent when viewed in different directions. The *Mercury* aromatics analyser indicates two strong (d = 5.09 Å) interactions between phenyl rings, three moderate (d = 5.89, 5.89, and 6.32 Å), and some weaker interactions (d > 8.7 Å). Analysis of the contributions to the total crystal energy of the structure using the Forcite module of *Materials Studio* (Dassault Systèmes, 2025) indicated that the intramolecular energy is dominated by angle distortion terms, and that bond and torsion terms are also significant. The intermolecular energy is dominated by van der Waals attractions, which in this force

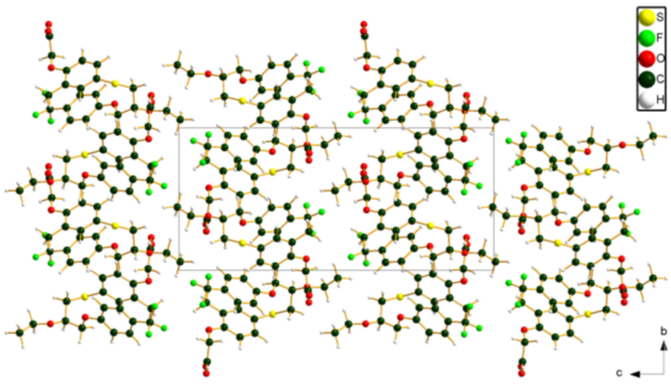

Figure 5
Crystal structure of seladelpar, viewed down the *a*-axis direction.

Table 1
Selected torsion angles (°).

C13—S1—C11—C10	−89.2	C11—C10—O5—C14	75.6
S1—C11—C10—C12	60.4	C10—O5—C14—C21	162.4
O5—C10—C11—S1	−177.7	C10—C12—O6—C15	−169.8
C17—C13—S1—C11	125.4	O5—C10—C12—O6	−64.9
C18—C13—S1—C11	−58.4	C19—O7—C29—C30	−82.2
C11—C10—C12—O6	58.8		

field-based analysis include hydrogen bonds. The hydrogen bonds are better discussed using the results of the DFT calculation.

There is one classical O—H···O hydrogen bond in the structure (Table 2). The energy of this bond (14.7 kcal mol^{-1}) was calculated using the correlation of Rammohan & Kaduk (2018). This links the carboxylic acid and the ether O5 atom into chains propagating along the *b*-axis direction, with graph-set motif (Etter, 1990; Bernstein *et al.*, 1995; Motherwell *et al.*, 2000) *C*(13). A less-traditional (and from the overlap population, surprisingly strong) C—H···S hydrogen bond links an aromatic ring and the S atom, and reinforces the chains along the *b*-axis.

The volume enclosed by the Hirshfeld surface of seladelpar (Fig. 6; Hirshfeld, 1977; Spackman *et al.*, 2021) is 546.7 Å^3 or 98.6% of 1/4 of the unit cell volume. The packing density is thus typical. The close contacts (red in Fig. 6) involve the hydrogen bonds. The volume per non-hydrogen atom is normal, at 18.5 Å^3.

The Bravais–Friedel–Donnay–Harker (Bravais, 1866; Friedel, 1907; Donnay & Harker, 1937) algorithm suggests that we might expect lozenge morphology for seladelpar, with {001} as the major faces. A second-order spherical harmonic model for preferred orientation was included. The texture index was 1.006, indicating that the preferred orientation was negligible in this rotated capillary specimen.

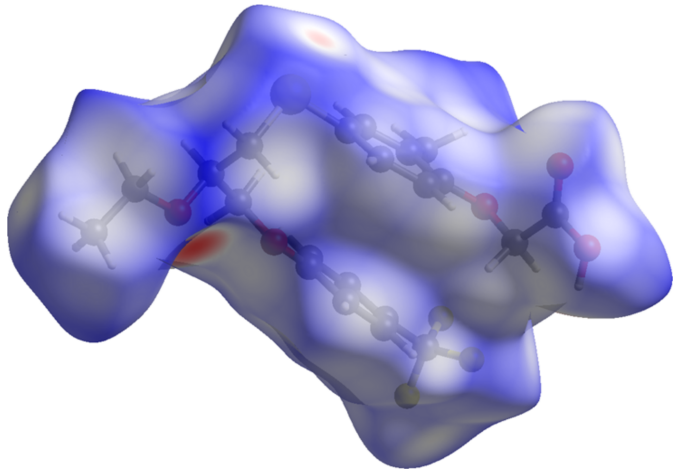

Figure 6
The Hirshfeld surface of seladelpar. Intermolecular contacts longer than the sums of the van der Waals radii are colored blue, and contacts shorter than the sums of the radii are colored red. Contacts approximately equal to the sums of radii are white.

4. Database survey

Powder diffraction data for anhydrous and dihydrate lysine salts of seladelpar are reported in US Patent US 7,709,682 B2 (Abdel-Magid *et al.*, 2010; Janssen Pharmaceutical). We are unaware of any published powder diffraction data for seladelpar itself. The structures of several proteins complexed with seladelpar, have been determined (Kamata *et al.*, 2023; PDB entries 8HUN, 8HUO, and 8HUP). A reduced cell search in the Cambridge Structural Database (Groom *et al.*, 2016), with the chemistry C, H, F, O and S only, yielded no hits.

5. Synthesis and crystallization

Seladelpar is a commercial reagent, purchased from TargetMol (Batch #225397), and was used as-received.

6. Refinement

Crystal data, data collection and structure refinement details are summarized in Table 3. The white powder was packed into a 1.5 mm diameter Kapton capillary, and rotated during the measurement at 50 Hz. The powder pattern was measured at 295 K at beam line 11-BM (Lee *et al.*, 2008; Wang *et al.*, 2008; Antao *et al.*, 2008) of the Advanced Photon Source at Argonne National Laboratory using a wavelength of 0.4687342 Å from 0.5–50° 2θ with a step size of 0.001° and a counting time of 0.1 sec step^{-1}. The high-resolution powder diffraction data were collected using twelve silicon crystal analyzers that allow for high angular resolution, high precision, and accurate peak positions. A mixture of silicon (NIST SRM 640c) and alumina (NIST SRM 676a) standards (ratio Al_2O_3:Si = 2:1 by weight) was used to calibrate the instrument and refine the monochromatic wavelength used in the experiment.

The pattern was indexed on a primitive orthorhombic unit cell with a = 8.87586, b = 10.62254, c = 23.54278 Å, V = 2219.7 Å^3, and Z = 4 using *N-TREOR* as incorporated into *EXPO2014* (Altomare *et al.*, 2013). The suggested space group was $P2_12_12_1$, which was confirmed by the successful solution and refinement of the structure. This cell does not account for a few weak peaks, so the sample contains at least one crystalline impurity.

The molecular structure of seladelpar was downloaded from PubChem (Kim *et al.*, 2023) as Conformer3D_COMPOUND_CID_11236126.sdf. It was converted to a *.mol2 file using *Mercury* (Macrae *et al.*, 2020), and to a Fenske–Hall *Z*-matrix using *OpenBabel* (O'Boyle *et al.*, 2011). The structure was solved using parallel tempering techniques as implemented in *FOX* (Favre-Nicolin & Černý, 2002).

Rietveld refinement was carried out using *GSAS-II* (Toby & Von Dreele, 2013). Only the 1.5–19.0° portion of the pattern was included in the refinements (d_{min} = 1.420 Å). All non-H bond distances and angles were subjected to restraints, based on a *Mercury*/Mogul Geometry Check (Sykes *et al.*, 2011; Bruno *et al.*, 2004). The Mogul average and standard deviation for each quantity were used as the restraint parameters. The aromatic rings were restrained to be planar. The restraints contributed 7.3% to the overall χ^2. The hydrogen atoms were included in calculated positions, which were recalculated during the refinement using Mercury. The U_{iso} values of the non-H atoms were grouped by chemical similarity. The U_{iso} of the H atoms were fixed at 1.2× the U_{iso} of the heavy atom to which they are attached. The peak profiles were described using the generalized microstrain model (Stephens, 1999). The background was modeled using a six-term shifted Chebyshev polynomial, with a peak at 6.08° to model the scattering from the Kapton capillary and any amorphous component of the sample.

The final refinement of 114 variables using 17,501 observations and 75 restraints yielded the residuals R_{wp} = 0.0914

Table 3
Experimental details.

Crystal data	
Chemical formula	$C_{21}H_{23}F_3O_5S$
M_r	444.46
Crystal system, space group	Orthorhombic, $P2_12_12_1$
Temperature (K)	295
a, b, c (Å)	8.85689 (7), 10.62563 (8), 23.57851 (14)
V (Å^3)	2218.98 (2)
Z	4
Radiation type	Synchrotron, λ = 0.46873 Å
μ (mm^{-1})	0.02
Specimen shape, size (mm)	Cylinder, 2.0 × 1.5
Data collection	
Diffractometer	11-BM, APS
Specimen mounting	Kapton capillary
Data collection mode	Transmission
Scan method	Step
2θ values (°)	$2\theta_{min}$ = 0.510, $2\theta_{max}$ = 49.995, $2\theta_{step}$ = 0.001
Refinement	
R factors and goodness of fit	R_p = 0.066, R_{wp} = 0.088, R_{exp} = 0.027, $R(F^2)$ = 0.06486, χ^2 = 11.169
No. of parameters	114
No. of restraints	75
$(\Delta/\sigma)_{max}$	11.051

Computer programs: *GSAS-II* (Toby & Von Dreele, 2013).

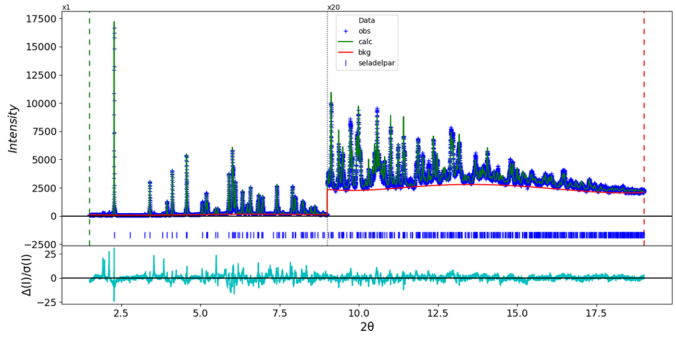

Figure 7
The Rietveld plot for seladelpar. The blue crosses represent the observed data points, and the green line is the calculated pattern. The cyan curve is the normalized error plot, and the red line is the background curve. The blue tick marks indicate the peak positions. The vertical scale has been multiplied by a factor of 20× for 2θ > 9.0°.

and GOF = 3.34. The largest peak (1.21 Å from F4) and hole (1.95 Å from S1) in the difference-Fourier map are 0.23 (4) and −0.20 (4) *e* Å^{-3}, respectively. The final Rietveld plot is shown in Fig. 7. The largest features in the normalized error plot are at the impurity peaks and in the shape of the lowest-angle 002 peak.

The crystal structure of seladelpar was optimized (fixed experimental unit cell) with density functional theory techniques using *VASP* (Kresse & Furthmüller, 1996) through the *MedeA* graphical interface (Materials Design, 2024). The calculation was carried out on 32 cores of a 144-core (768 Gb memory) HPE Superdome Flex 280 Linux server at North Central College. The calculation used the GGA-PBE functional, a plane wave cutoff energy of 400.0 eV, and a *k*-point spacing of 0.5 Å^{-1} leading to a 2 × 2 × 1 mesh, and took ∼11.9 h. Single-point density functional theory calculations (fixed experimental cell) and population analysis were carried out using *CRYSTAL23* (Erba *et al.*, 2023). (fixed experimental cell) and population analysis were carried out using *CRYSTAL17* (Dovesi *et al.*, 2018). The basis sets for the H, C, and O atoms in the calculation were those of Gatti *et al.* (1994), and those for F and S were from Peintinger *et al.* (2013). The calculations were run on a 3.5 GHz PC using 8 *k*-points and the B3LYP functional, and took ∼3.2 h. The powder pattern has been submitted to ICDD for inclusion in the Powder Diffraction File (PDF).

Acknowledgements

Use of the Advanced Photon Source at Argonne National Laboratory was supported by the US Department of Energy, Office of Science, Office of Basic Energy Sciences, under Contract No. DE-AC02–06CH11357. We thank Saul Lapidus for his assistance in the data collection. We also thank the ICDD team – Steve Trimble, and Dave Bohnenberger – for their contribution to research, sample preparation, and in-house XRD data collection and verification.

Funding information

Funding for this research was provided by: International Centre for Diffraction Data (grant No. 09-03).

References

Abdel-Magid, A. F., Mehrman, S. J. & Roessier, A. (2010). United States Patent US 7,709,682 B2.
Altomare, A., Cuocci, C., Giacovazzo, C., Moliterni, A., Rizzi, R., Corriero, N. & Falcicchio, A. (2013). *J. Appl. Cryst.* **46**, 1231–1235.
Antao, S. M., Hassan, I., Wang, J., Lee, P. L. & Toby, B. H. (2008). *Can. Mineral.* **46**, 1501–1509.
Bernstein, J., Davis, R. E., Shimoni, L. & Chang, N. L. (1995). *Angew. Chem. Int. Ed. Engl.* **34**, 1555–1573.
Bravais, A. (1866). *Etudes Cristallographiques.* Paris: Gauthier Villars.
Bruno, I. J., Cole, J. C., Kessler, M., Luo, J., Motherwell, W. D. S., Purkis, L. H., Smith, B. R., Taylor, R., Cooper, R. I., Harris, S. E. & Orpen, A. G. (2004). *J. Chem. Inf. Comput. Sci.* **44**, 2133–2144.
Dassault Systèmes. (2025). *BIOVIA Materials Studio 2025*. BIOVIA, San Diego, CA, USA.
Dovesi, R., Erba, A., Orlando, R., Zicovich-Wilson, C. M., Civalleri, B., Maschio, L., Rérat, M., Casassa, S., Baima, J., Salustro, S. & Kirtman, B. (2018). *WIREs Comput. Mol. Sci.* **8**, e1360.
Donnay, J. D. H. & Harker, D. (1937). *Am. Mineral.* **22**, 446–467.
Erba, A., Desmarais, J. K., Casassa, S., Civalleri, B., Donà, L., Bush, I. J., Searle, B., Maschio, L., Edith-Daga, L., Cossard, A., Ribaldone, C., Ascrizzi, E., Marana, N. L., Flament, J.-P. & Kirtman, B. (2023). *J. Chem. Theory Comput.* **19**, 6891–6932.
Etter, M. C. (1990). *Acc. Chem. Res.* **23**, 120–126.
Favre-Nicolin, V. & Černý, R. (2002). *J. Appl. Cryst.* **35**, 734–743.
Friedel, G. (1907). *Bull. Soc. Fr. Minéral.* **30**, 326–455.
Gatti, C., Saunders, V. R. & Roetti, C. (1994). *J. Chem. Phys.* **101**, 10686–10696.
Groom, C. R., Bruno, I. J., Lightfoot, M. P. & Ward, S. C. (2016). *Acta Cryst.* B**72**, 171–179.
Hirshfeld, F. L. (1977). *Theoret. Chem. Acta* **44**, 129-138.
Kabekkodu, S., Dosen, A. & Blanton, T. N. (2024). *Powder Diffr.* **39**, 47–59.
Kaduk, J. A., Crowder, C. E., Zhong, K., Fawcett, T. G. & Suchomel, M. R. (2014). *Powder Diffr.* **29**, 269–273.
Kamata, S., Honda, A., Ishikawa, R., Akahane, M., Fujita, A., Kaneko, C., Miyawaki, S., Shiiyama, Y., Machida, K., Oyama, T. & Ishii, I. (2023). *antioxidants* **12**, 1523.
Kim, S., Chen, J., Cheng, T., Gindulyte, A., He, J., He, S., Li, Q., Shoemaker, B. A., Thiessen, P. A., Yu, B., Zaslavsky, L., Zhang, J. & Bolton, E. E. (2023). *Nucleic Acids Res.* **51**, D1373–D1380.
Kresse, G. & Furthmüller, J. (1996). *Comput. Mater. Sci.* **6**, 15–50.
Lee, P. L., Shu, D., Ramanathan, M., Preissner, C., Wang, J., Beno, M. A., Von Dreele, R. B., Ribaud, L., Kurtz, C., Antao, S. M., Jiao, X. & Toby, B. H. (2008). *J. Synchrotron Rad.* **15**, 427–432.
Macrae, C. F., Sovago, I., Cottrell, S. J., Galek, P. T. A., McCabe, P., Pidcock, E., Platings, M., Shields, G. P., Stevens, J. S., Towler, M. & Wood, P. A. (2020). *J. Appl. Cryst.* **53**, 226–235.
Materials Design. (2024). *MedeA* Version 3.7.2. Materials Design Inc., San Diego, USA.
Motherwell, W. D. S., Shields, G. P. & Allen, F. H. (2000). *Acta Cryst.* B**56**, 857–871.
O'Boyle, N. M., Banck, M., James, C. A., Morley, C., Vandermeersch, T. & Hutchison, G. R. (2011). *J. Chem. Informatics* **3**, 33.
Peintinger, M. F., Oliveira, D. V. & Bredow, T. (2013). *J. Comput. Chem.* **34**, 451–459.
Rammohan, A. & Kaduk, J. A. (2018). *Acta Cryst.* B**74**, 239–252.
Shukla, A. K. & Misra, S. (2025). *J. Basic Clin. Physiol. Pharmacol.* **36**, 331–337.
Spackman, P. R., Turner, M. J., McKinnon, J. J., Wolff, S. K., Grimwood, D. J., Jayatilaka, D. & Spackman, M. A. (2021). *J. Appl. Cryst.* **54**, 1006–1011.
Stephens, P. W. (1999). *J. Appl. Cryst.* **32**, 281–289.
Streek, J. van de & Neumann, M. A. (2014). *Acta Cryst.* B**70**, 1020–1032.
Sykes, R. A., McCabe, P., Allen, F. H., Battle, G. M., Bruno, I. J. & Wood, P. A. (2011). *J. Appl. Cryst.* **44**, 882–886.
Toby, B. H. & Von Dreele, R. B. (2013). *J. Appl. Cryst.* **46**, 544–549.
Wang, J., Toby, B. H., Lee, P. L., Ribaud, L., Antao, S. M., Kurtz, C., Ramanathan, M., Von Dreele, R. B. & Beno, M. A. (2008). *Rev. Sci. Instrum.* **79**, 085105.
Wavefunction (2025). *Spartan '24.* Version 1.3.1. Wavefunction Inc., Irvine, USA.

supporting information

Acta Cryst. (2026). E**82** [https://doi.org/10.1107/S2056989026007875]

Crystal structure of seladelpar, $C_{21}H_{23}F_3O_5S$, from synchrotron powder diffraction data and density functional theory

Jacob K. Salazar, James A. Kaduk, Anja Dosen, Megan Rost and Thomas N. Blanton

Computing details

2-(4-{(2*R*)-2-Ethoxy-3-[4-(trifluoromethyl)phenoxy]propylsulfanyl}-2-methylphenoxy)acetic acid (seladelpar)

Crystal data

$C_{21}H_{23}F_3O_5S$
M_r = 444.46
Orthorhombic, $P2_12_12_1$
a = 8.85689 (7) Å
b = 10.62563 (8) Å
c = 23.57851 (14) Å
V = 2218.98 (2) Å^3
Z = 4
D_x = 1.330 Mg m^{-3}
Synchrotron radiation, λ = 0.46873 Å
μ = 0.02 mm^{-1}
T = 295 K
cylinder, 2.0 × 1.5 mm

Data collection

11-BM, APS diffractometer
Specimen mounting: Kapton capillary
Data collection mode: transmission
Scan method: step
$2\theta_{min}$ = 0.510°, $2\theta_{max}$ = 49.995°, $2\theta_{step}$ = 0.001°

Refinement

Least-squares matrix: full
R_p = 0.066
R_{wp} = 0.088
R_{exp} = 0.027
$R(F^2)$ = 0.06486
49486 data points
Profile function: Finger-Cox-Jephcoat function parameters U, V, W, X, Y, SH/L: peak variance(Gauss) = Utan(Th)^2+Vtan(Th)+W: peak HW(Lorentz) = X/cos(Th)+Ytan(Th); SH/L = S/L+H/L U, V, W in (centideg)^2, X & Y in centideg 1.163, -0.126, 0.063, 0.000, 0.000, 0.002,
114 parameters
75 restraints
25 constraints
Weighting scheme based on measured s.u.'s
$(\Delta/\sigma)_{max}$ = 11.051
Background function: Background function: "chebyschev-1" function with 6 terms: 83.2(15), 38.6(18), 1.6(7), -42.6(15), 20.8(9), 3.7(4), Background peak parameters: pos, int, sig, gam: 6.080(24), 7.1(3)e4, 3.46(12)e4, 0.100,
Preferred orientation correction: Simple spherical harmonic correction Order = 2 Coefficients: 0:0:C(2,0) = -0.1570; 0:0:C(2,2) = 0.0680

Fractional atomic coordinates and isotropic or equivalent isotropic displacement parameters (Å^2)

	x	*y*	*z*	U_{iso}*/U_{eq}
S1	−0.0693 (5)	0.8031 (4)	0.2987 (2)	0.090 (2)*
F2	0.7564 (9)	0.5457 (7)	0.0969 (4)	0.110 (2)*
F3	0.7032 (8)	0.7385 (6)	0.0780 (3)	0.110 (2)*

F4	0.5772 (9)	0.5866 (7)	0.0556 (3)	0.110 (2)*
O5	0.2116 (8)	0.6317 (8)	0.4072 (4)	0.074 (2)*
O6	0.3274 (10)	0.6649 (8)	0.2992 (4)	0.074 (2)*
O7	0.3205 (9)	0.9186 (8)	0.0999 (3)	0.091 (2)*
O8	0.4964 (8)	1.2284 (8)	0.0955 (5)	0.091 (2)*
O9	0.2451 (9)	1.1752 (7)	0.0908 (5)	0.091 (2)*
C10	0.1126 (10)	0.6346 (9)	0.3592 (4)	0.074 (2)*
C11	0.0640 (11)	0.7684 (10)	0.3557 (4)	0.074 (2)*
C12	0.1936 (12)	0.5916 (10)	0.3060 (4)	0.074 (2)*
C13	0.0490 (9)	0.8496 (9)	0.2404 (3)	0.038 (3)*
C14	0.1323 (11)	0.6125 (11)	0.4623 (5)	0.074 (2)*
C15	0.4075 (14)	0.6504 (12)	0.2525 (4)	0.110 (2)*
C16	0.1267 (10)	0.8081 (8)	0.1427 (3)	0.038 (3)*
C17	0.0330 (9)	0.7833 (8)	0.1890 (4)	0.038 (3)*
C18	0.1583 (11)	0.9472 (8)	0.2440 (3)	0.038 (3)*
C19	0.2459 (13)	0.8937 (11)	0.1496 (3)	0.038 (3)*
C20	0.2492 (11)	0.9734 (9)	0.1961 (4)	0.038 (3)*
C21	0.2342 (15)	0.5533 (13)	0.4997 (5)	0.074 (2)*
C22	0.5226 (13)	0.7313 (10)	0.2432 (4)	0.110 (2)*
C23	0.3515 (14)	0.5777 (12)	0.2093 (4)	0.110 (2)*
C24	0.5616 (11)	0.6439 (11)	0.1505 (4)	0.110 (2)*
C25	0.1227 (10)	0.7196 (8)	0.0935 (4)	0.038 (3)*
C26	0.5977 (12)	0.7303 (11)	0.1910 (4)	0.110 (2)*
C27	0.4405 (10)	0.5645 (11)	0.1606 (3)	0.110 (2)*
C28	0.6537 (8)	0.6326 (6)	0.0973 (3)	0.110 (2)*
C29	0.4303 (10)	1.0128 (8)	0.0970 (5)	0.091 (2)*
C30	0.3809 (9)	1.1448 (7)	0.0919 (8)	0.091 (2)*
H1	0.59404	1.18258	0.09406	0.1095*
H2	0.01509	0.57462	0.36702	0.0882*
H3	0.16412	0.82616	0.34929	0.0882*
H4	0.01101	0.79351	0.39581	0.0882*
H5	0.22332	0.49253	0.30988	0.0882*
H6	0.12036	0.60460	0.26937	0.0882*
H7	0.09737	0.70291	0.47965	0.0882*
H8	0.03346	0.55313	0.45607	0.0882*
H9	−0.05405	0.71139	0.18531	0.0453*
H10	0.17186	1.00095	0.28299	0.0453*
H11	0.32173	1.05616	0.19577	0.0453*
H12	0.33292	0.61300	0.50555	0.0882*
H13	0.26901	0.46322	0.48197	0.0882*
H14	0.17938	0.53796	0.54046	0.0882*
H15	0.55678	0.79704	0.27622	0.1322*
H16	0.24187	0.53194	0.21275	0.1322*
H17	0.02154	0.66162	0.09621	0.0453*
H18	0.22226	0.65950	0.09449	0.0453*
H19	0.12138	0.77315	0.05412	0.0453*
H20	0.68590	0.79927	0.18265	0.1322*
H21	0.41411	0.49062	0.13016	0.1322*

H22	0.49806	1.00599	0.13542	0.1095*
H23	0.50063	0.99235	0.06025	0.1095*

Geometric parameters (Å, º)

S1—C11	1.826 (6)	C21—C14	1.410 (14)
S1—C13	1.798 (5)	C21—H12	1.089 (13)
F2—F3	2.149 (9)	C21—H13	1.088 (13)
F2—F4	1.912 (9)	C21—H14	1.090 (13)
F2—C28	1.296 (8)	C22—C15	1.352 (6)
F3—F2	2.149 (9)	C22—C26	1.399 (6)
F3—F4	2.032 (9)	C22—H15	1.089 (6)
F3—C28	1.291 (8)	C23—C15	1.371 (7)
F4—F2	1.912 (9)	C23—C27	1.399 (7)
F4—F3	2.032 (9)	C23—H16	1.089 (8)
F4—C28	1.290 (8)	C24—C26	1.362 (5)
O5—C10	1.431 (7)	C24—C27	1.385 (5)
O5—C14	1.491 (9)	C24—C28	1.502 (5)
O6—C12	1.428 (8)	C25—C16	1.494 (6)
O6—C15	1.319 (6)	C25—H17	1.089 (9)
O7—C19	1.370 (6)	C25—H18	1.089 (9)
O7—C29	1.397 (6)	C25—H19	1.089 (10)
O8—C30	1.357 (7)	C26—C22	1.399 (6)
O8—H1	0.993 (7)	C26—C24	1.362 (5)
O9—C30	1.246 (8)	C26—H20	1.089 (7)
C10—O5	1.431 (7)	C27—C23	1.399 (7)
C10—C11	1.488 (7)	C27—C24	1.385 (5)
C10—C12	1.516 (8)	C27—H21	1.090 (7)
C10—H2	1.089 (9)	C28—F2	1.296 (8)
C11—S1	1.826 (6)	C28—F3	1.291 (8)
C11—C10	1.488 (7)	C28—F4	1.290 (8)
C11—H3	1.089 (11)	C28—C24	1.502 (5)
C11—H4	1.088 (10)	C29—O7	1.397 (6)
C12—O6	1.428 (8)	C29—C30	1.474 (7)
C12—C10	1.516 (8)	C29—H22	1.089 (12)
C12—H5	1.089 (11)	C29—H23	1.089 (10)
C12—H6	1.089 (11)	C30—O8	1.357 (7)
C13—S1	1.798 (5)	C30—O9	1.246 (8)
C13—C17	1.409 (5)	C30—C29	1.474 (7)
C13—C18	1.421 (6)	H1—O8	0.993 (7)
C14—O5	1.491 (9)	H2—C10	1.089 (9)
C14—C21	1.410 (14)	H3—C11	1.089 (11)
C14—H7	1.089 (11)	H4—C11	1.088 (10)
C14—H8	1.089 (11)	H5—C12	1.089 (11)
C15—O6	1.319 (6)	H6—C12	1.089 (11)
C15—C22	1.352 (6)	H7—C14	1.089 (11)
C15—C23	1.371 (7)	H8—C14	1.089 (11)
C16—C17	1.396 (4)	H9—C17	1.089 (6)

C16—C19	1.403 (6)	H10—C18	1.089 (7)
C16—C25	1.494 (6)	H11—C20	1.089 (7)
C17—C13	1.409 (5)	H12—C21	1.089 (13)
C17—C16	1.396 (4)	H13—C21	1.088 (13)
C17—H9	1.089 (6)	H14—C21	1.090 (13)
C18—C13	1.421 (6)	H15—C22	1.089 (6)
C18—C20	1.414 (6)	H16—C23	1.089 (8)
C18—H10	1.089 (7)	H17—C25	1.089 (9)
C19—O7	1.370 (6)	H18—C25	1.089 (9)
C19—C16	1.403 (6)	H19—C25	1.089 (10)
C19—C20	1.387 (6)	H20—C26	1.089 (7)
C20—C18	1.414 (6)	H21—C27	1.090 (7)
C20—C19	1.387 (6)	H22—C29	1.089 (12)
C20—H11	1.089 (7)	H23—C29	1.089 (10)

C11—S1—C13	104.0 (4)	C16—C19—C20	120.2 (4)
C10—O5—C14	113.8 (5)	C18—C20—C19	120.0 (4)
C12—O6—C15	118.4 (6)	C18—C20—H11	120.1 (7)
C19—O7—C29	121.1 (6)	C19—C20—H11	119.9 (7)
C30—O8—H1	109.5 (7)	C14—C21—H12	109.5 (12)
O5—C10—C11	104.0 (6)	C14—C21—H13	109.5 (11)
O5—C10—C12	110.9 (7)	H12—C21—H13	109.5 (11)
C11—C10—C12	112.3 (7)	C14—C21—H14	109.4 (11)
O5—C10—H2	109.9 (7)	H12—C21—H14	109.4 (11)
C11—C10—H2	109.8 (9)	H13—C21—H14	109.5 (12)
C12—C10—H2	109.8 (8)	C15—C22—C26	119.7 (3)
S1—C11—C10	114.9 (6)	C15—C22—H15	120.1 (7)
S1—C11—H3	108.1 (6)	C26—C22—H15	120.1 (7)
C10—C11—H3	108.1 (8)	C15—C23—C27	117.5 (5)
S1—C11—H4	108.1 (7)	C15—C23—H16	121.3 (8)
C10—C11—H4	108.1 (8)	C27—C23—H16	121.2 (7)
H3—C11—H4	109.5 (8)	C26—C24—C27	118.1 (3)
O6—C12—C10	108.8 (6)	C26—C24—C28	120.8 (4)
O6—C12—H5	109.6 (10)	C27—C24—C28	121.1 (4)
C10—C12—H5	109.7 (9)	C16—C25—H17	109.3 (6)
O6—C12—H6	109.6 (10)	C16—C25—H18	109.4 (9)
C10—C12—H6	109.7 (8)	H17—C25—H18	109.5 (8)
H5—C12—H6	109.5 (7)	C16—C25—H19	109.5 (8)
S1—C13—C17	117.5 (5)	H17—C25—H19	109.7 (8)
S1—C13—C18	123.5 (6)	H18—C25—H19	109.5 (7)
C17—C13—C18	119.0 (3)	C22—C26—C24	120.7 (4)
O5—C14—C21	107.7 (8)	C22—C26—H20	119.7 (6)
O5—C14—H7	109.9 (11)	C24—C26—H20	119.7 (7)
C21—C14—H7	109.9 (10)	C23—C27—C24	121.1 (4)
O5—C14—H8	109.9 (8)	C23—C27—H21	119.5 (6)
C21—C14—H8	109.9 (12)	C24—C27—H21	119.4 (6)
H7—C14—H8	109.5 (9)	F2—C28—F3	112.4 (6)
O6—C15—C22	117.8 (6)	F2—C28—F4	95.3 (6)

O6—C15—C23	119.5 (7)	F3—C28—F4	103.8 (6)
C22—C15—C23	120.7 (4)	F2—C28—C24	116.4 (6)
C17—C16—C19	118.6 (3)	F3—C28—C24	114.2 (5)
C17—C16—C25	118.3 (4)	F4—C28—C24	112.4 (5)
C19—C16—C25	121.1 (4)	O7—C29—C30	118.6 (7)
C13—C17—C16	121.2 (3)	O7—C29—H22	107.1 (8)
C13—C17—H9	119.3 (6)	C30—C29—H22	107.1 (11)
C16—C17—H9	119.4 (6)	O7—C29—H23	107.1 (8)
C13—C18—C20	118.9 (4)	C30—C29—H23	107.2 (11)
C13—C18—H10	120.6 (7)	H22—C29—H23	109.5 (8)
C20—C18—H10	120.5 (8)	O8—C30—O9	124.0 (6)
O7—C19—C16	112.9 (5)	O8—C30—C29	113.2 (6)
O7—C19—C20	123.2 (6)	O9—C30—C29	122.3 (6)

(seladelpar_VASP)

Crystal data

$C_{21}H_{23}F_3O_5S$
M_r = 444.46
Orthorhombic, $P2_12_12_1$
a = 8.85689 Å
b = 10.62563 Å
c = 23.57851 Å
V = 2218.97 Å^3
Z = 4

Data collection

$h = \rightarrow$
$k = \rightarrow$
$l = \rightarrow$

Fractional atomic coordinates and isotropic or equivalent isotropic displacement parameters (Å^2)

	x	y	z	B_{iso}*/B_{eq}
S1	−0.06226	0.81067	0.29800	
F2	0.77456	0.54746	0.09473	
F3	0.71686	0.74416	0.07619	
F4	0.56934	0.59128	0.04659	
O5	0.21714	0.62095	0.40710	
O6	0.32888	0.66722	0.29666	
O7	0.31495	0.92206	0.09562	
O8	0.50360	1.22795	0.08729	
O9	0.25766	1.17937	0.08604	
C10	0.11756	0.64131	0.35934	
C11	0.06945	0.77962	0.35565	
C12	0.19659	0.59245	0.30683	
C13	0.05734	0.84570	0.23965	
C14	0.14147	0.61905	0.46174	
C15	0.40328	0.65185	0.24652	
C16	0.12593	0.80438	0.14067	
C17	0.04109	0.77718	0.18907	
C18	0.16162	0.94442	0.24135	
C19	0.23206	0.90300	0.14406	
C20	0.24941	0.97255	0.19398	

C21	0.24516	0.55791	0.50448
C22	0.52414	0.73468	0.23699
C23	0.36658	0.56059	0.20585
C24	0.56755	0.63829	0.14545
C25	0.11139	0.72919	0.08716
C26	0.60502	0.72797	0.18674
C27	0.44978	0.55388	0.15579
C28	0.65496	0.63091	0.09138
C29	0.43670	1.00800	0.09718
C30	0.38886	1.14525	0.08996
H1	0.60569	1.18687	0.09182
H2	0.01570	0.58277	0.36528
H3	0.16772	0.84182	0.35156
H4	0.00738	0.80551	0.39423
H5	0.22856	0.49313	0.31316
H6	0.11867	0.59834	0.27056
H7	0.11314	0.71583	0.47476
H8	0.03500	0.56616	0.45721
H9	−0.03852	0.69872	0.18759
H10	0.17493	1.00072	0.27971
H11	0.32779	1.05128	0.19648
H12	0.35153	0.61041	0.50867
H13	0.26913	0.45973	0.49293
H14	0.19102	0.55929	0.54627
H15	0.55108	0.80474	0.26919
H16	0.27245	0.49580	0.21180
H17	0.02872	0.65325	0.09216
H18	0.22091	0.68798	0.07532
H19	0.07661	0.78864	0.05126
H20	0.69791	0.79322	0.17921
H21	0.42195	0.48166	0.12463
H22	0.50381	0.99822	0.13638
H23	0.51065	0.98199	0.06162

Torsion angles (º)

C13—S1—C11—C10	−89.2	C11—C10—O5—C14	75.6
S1—C11—C10—C12	60.4	C10—O5—C14—C21	162.4
O5—C10—C11—S1	−177.7	C10—C12—O6—C15	−169.8
C17—C13—S1—C11	125.4	O5—C10—C12—O6	−64.9
C18—C13—S1—C11	−58.4	C19—O7—C29—C30	−82.2
C11—C10—C12—O6	58.8		

Hydrogen-bond geometry (Å, º)

D—H···*A*	*D*—H	H···*A*	*D*···*A*	*D*—H···*A*
O8—H1···O5^{i}	1.01	1.72	2.725	175

C23—H16···S1^{ii}	1.09	2.72	3.785	166

Symmetry codes: (i) −*x*+1, *y*+1/2, −*z*+1/2; (ii) −*x*, *y*−1/2, −*z*+1/2.